ACS APPLIED MATERIALS & INTERFACES

Research Article

www.acsami.org

Antiviral Activity of Graphene Oxide: How Sharp Edged Structure and Charge Matter

Shiyi Ye,[†] Kang Shao,[†] Zhonghua Li,[†] Nan Guo,[‡] Yunpeng Zuo,[†] Qin Li,[†] Zhicheng Lu,[†] Lu Chen,[†] Qigai He,[*,‡] and Heyou Han[*,†]

[†]State Key Laboratory of Agricultural Microbiology, College of Science and [‡]Division of Animal Infectious Disease, College of Veterinary Medicine, Huazhong Agricultural University, Wuhan 430070, P.R. China

Supporting Information

ABSTRACT: Graphene oxide and its derivatives have been widely explored for their antimicrobial properties due to their high surface-to-volume ratios and unique chemical and physical properties. However, little information is available on their effects on viruses. In this study, we report the broad-spectrum antiviral activity of GO against pseudorabies virus (PRV, a DNA virus) and porcine epidemic diarrhea virus (PEDV, an RNA virus). Our results showed that GO significantly suppressed the infection of PRV and PEDV for a 2 log reduction in virus titers at noncytotoxic concentrations. The potent antiviral activity of both GO and rGO can be attributed to the unique single-layer structure and negative charge. First, GO exhibited potent antiviral activity when conjugated with PVP, a nonionic polymer, but not when conjugated with PDDA, a cationic polymer. Additionally, the precursors Gt and GtO showed much weaker antiviral activity than monolayer GO and rGO, suggesting that the nanosheet structure is important for antiviral properties. Furthermore, GO inactivated both viruses by structural destruction prior to viral entry. The overall results suggest the potential of graphene oxide as a novel promising antiviral agent with a broad and potent antiviral activity.

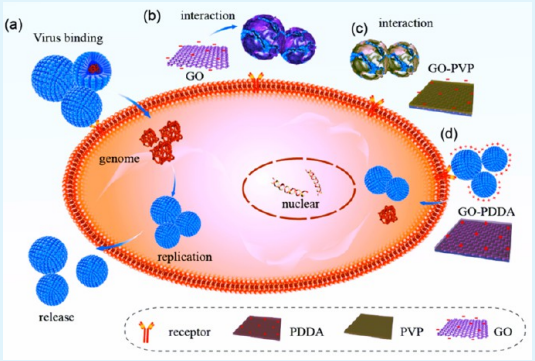

KEYWORDS: *graphene oxide, antivirus, reduced graphene oxide, porcine epidemic diarrhea virus, pseudorabies virus*

1. INTRODUCTION

Infectious diseases caused by viruses constantly threaten the health of both humans and animals. Although some viral diseases have been alleviated or even eradicated by vaccination, such as smallpox,[1] some are not controlled. Low cross-protection among different serotypes[2,3] and variation between numerous strains[4,5] hamper prophylaxis of these viral infections, and a viricide is extremely needed to inactivate the virus in the environment.

Pseudorabies virus (PRV) is an alpha-herpesvirus containing a double stranded DNA genome and can infect most species of mammals, causing various lesions mainly in the central nervous system, respiratory system, or reproductive system.[6] Pseudorabies has been effectively controlled by vaccination for nearly 30 years. However, it reemerged in immunized farms in China around 2011 because of antigenic variation.[7,8] Porcine epidemic diarrhea virus (PEDV) is a positive-strand RNA virus belonging to alpha-coronavirus. It is the most important agent of viral diarrhea, causing severe economic losses to the pig industry worldwide due to high mortality in piglets.[9,10] Inactivated and attenuated vaccines are available for PRV and PEDV, but these diseases are still frequently noted in the livestock industry, partly because of the emergence of new variant strains. So far, no specific antiviral therapeutic is available for these viral infections. With the risk of emerging or re-emerging diseases, there is an urgent need to develop novel antimicrobial compounds.

Currently, nanoscale materials have emerged as novel "antimicrobial agents" due to their high surface area to volume ratio and their unique chemical and physical properties.[11−15] Graphene oxide is a two-dimensional crystal structure characterized by a single atomic thick sheet formed by carbon atoms arranged in a hexagonal lattice.[16] The oxygen-containing functional groups and the unique physicochemical properties facilitate their applications in bioengineering. The apparently low toxicity enabled these GO materials to be promising candidates for the next generation of antimicrobial agents. Studies have shown that graphene oxide and its derivatives exhibit broad-spectrum inhibition activity against bacteria[17,18] and fungi.[19,20] Recently, Sametband et al. reported that GO and partially reduced sulfonated GO could inhibit HSV-1 infection through cell attachment inhibition at low concentrations.[21] However, to date, their potential inhibitory effects on other viruses have not been reported, and the mechanism by which they influence viruses remains to be elucidated.

To better understand the impacts of graphene materials on viruses, we evaluated the antiviral properties of GO on both RNA and DNA virus models. To further reveal the antiviral mechanism, we adopted graphite (Gt) and graphite oxide

Received: July 28, 2015
Accepted: September 15, 2015
Published: September 15, 2015

DOI: 10.1021/acsami.5b06876
ACS Appl. Mater. Interfaces 2015, 7, 21571−21579

(GtO), which are precursors of GO and reduced GO (rGO), to test whether the layer structure was required in antiviral activity. The impact of charge was analyzed by examining whether GO conjugated with cationic polymer PDDA or nonionic PVP could exhibit potent antiviral activity. Additionally, the GO was added at different stages of viral infection to explore how GO affected the infection. In conclusion, we found that the negatively charged GO has more chances to interact with viruses through electrostatic interactions prior to viral entry, resulting in virus damage due to its single-layer structure and sharp edge (Scheme 1). Thus, GO may be a potential antiviral nanomaterial used as a therapeutic drug or environmental disinfectant.

Scheme 1. Possible Mechanisms of the Antiviral Activity of GO[a]

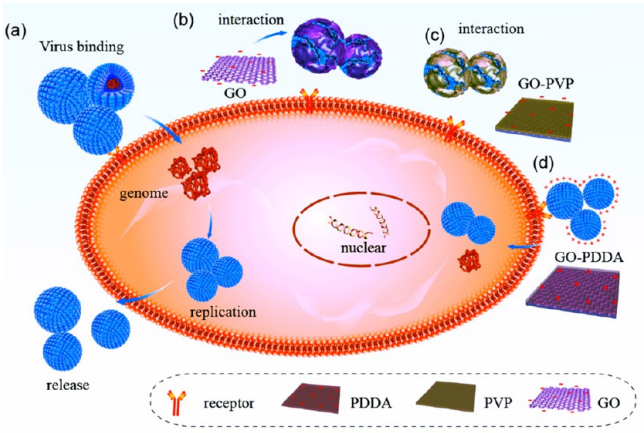

[a](a) Normal viruses are absorbed into cells by interacting with cell receptors to initiate infection. (b) Negatively charged GO has more chances to interact with the positively charged viruses, leading to virus damage and the inhibition of infection. (c) Infection was blocked by GO conjugated with nonionic PVP but not with cationic PDDA (d).

This study revealed the potent broad-spectrum activity of GO and proposes a potential mechanism (Scheme 1) that could facilitate a better understanding of GO applications and lay a basis for novel virucide development.

2. EXPERIMENTAL SECTION

2.1. Cells and Viruses. Vero cells and PK-15 cells were propagated in Dulbecco's modified Eagle medium (DMEM, Gibco, USA) supplemented with 10% fetal bovine serum in a 5% CO_2 incubator at 37 °C. A viral infection inhibition assay was performed with porcine epidemic diarrhea virus (PEDV) filed strain CH/YNKM-8/2013 (GenBank: KF761675.1), which was a DNA virus, and an RNA virus named pseudorabies virus filed strain HNX (GenBank: KM189912). These two viruses were both new variant strains that were isolated from infected pigs immunized with commercial vaccines.

2.2. Cytotoxicity Assay. Cytotoxicity of graphene oxide was assessed by MTT as previously described.[22] The Vero cells and PK-15 cells were seeded separately in a 96-well tissue culture plate. The cells were incubated with GO or rGO at different concentrations. After a 72 h incubation, 20 μL/well 3-(4,5-dimethyl-2-yl)-2,5-diphenyltetrazolium bromide (MTT, 5 mg/mL) was added and inoculated for 4 h. The liquid was removed, and 150 μL of DMSO was added to each well followed by a 10 min shake at room temperature. The absorbance was measured at a wavelength of 490 nm.

2.3. Plaque Reduction Assay. PEDV plaque reduction assay was performed on Vero cells while PRV was performed on PK-15 cells. The cells were inoculated on 12-well plates, PEDV or PRV (2000 pfu/well) was incubated with 6 μg/mL nanomaterials for 1 h at 37 °C, and then added to monolayer Vero cells or PK-15 cells at 60%−70% confluence. After 1 h viral adsorption, the cells were washed with DMEM and overlaid with sodium carboxymethyl cellulose containing medium supplemented with 8 μg/mL trypsin (PEDV) or 2% FBS (PRV). The plaques were fixed with 10% formaldehyde 3 days post infection and stained with crystal violet solution.[23]

2.4. Indirect Immunofluorescence Assay. Inhibitory effect of GO on cell infection by PEDV and PRV was further evaluated by immunofluorescence.[24] PK-15 (Vero) cells in 24-well plates were infected with PRV (PEDV) at 0.01 multiplicity of infection (MOI) in the presence or absence of GO. The cells were rinsed with PBS and fixed in 4% formaldehyde at room temperature for 15 min 24 h post infection. After permeabilization with 0.1% Triton X-100, the cells were incubated with the anti-PRV (PEDV) monoclonal antibody (1:500 dilution) for 1 h and fluorescein isothiocyanate (FITC)-conjugated goat antimouse antibody (1:60 dilution) for 1 h. Fluorescence micrographs were acquired on a Nikon Eclipse Ti microscope (Japan).

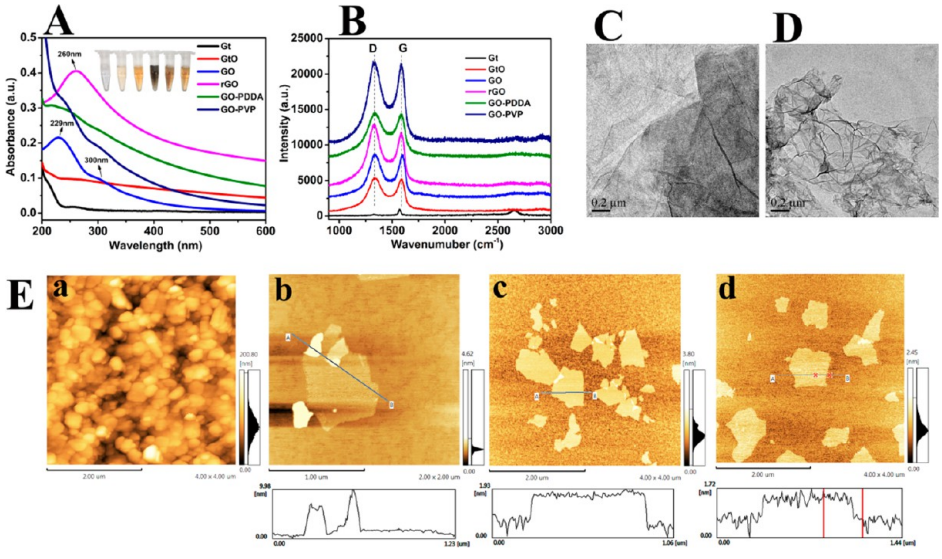

Figure 1. Characteristics of materials. (A) UV−vis absorption spectra photographs of the six materials in eppendorf tubes from left to right: Gt, GtO, GO, rGO, GO-PDDA, and GO-PVP. (B) Raman spectra of graphene-based materials. (C, D) TEM images of (C) GO and (D) rGO. (E) AFM analysis of Gt (a), GtO (b), GO (c), and rGO (d).

DOI: 10.1021/acsami.5b06876
ACS Appl. Mater. Interfaces 2015, 7, 21571−21579

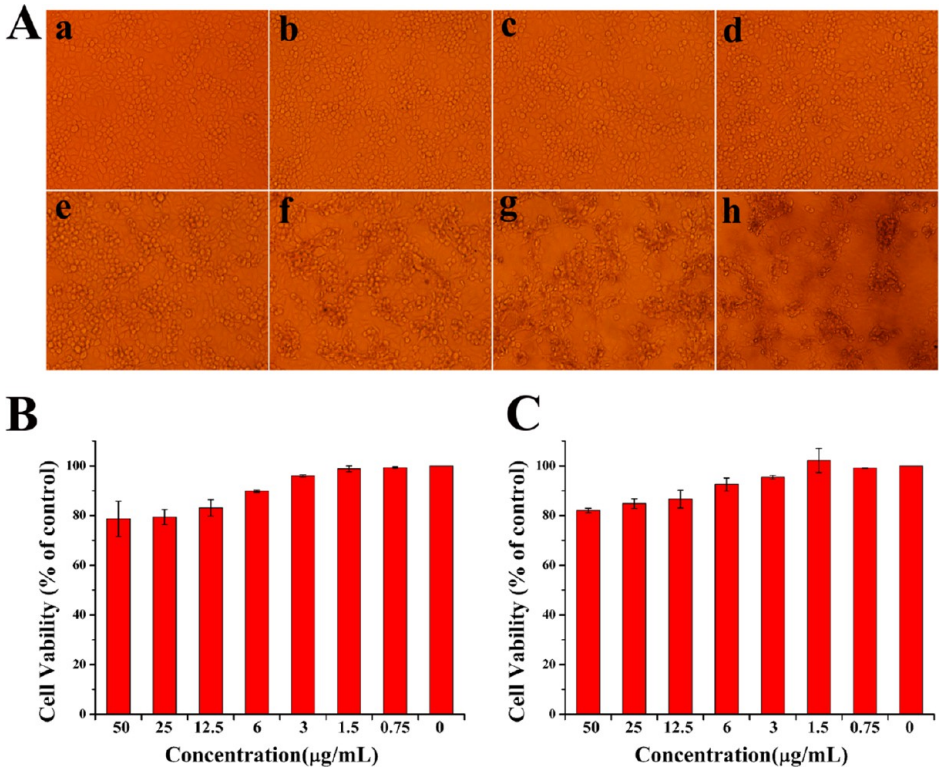

Figure 2. Cytotoxicity of graphene oxide on PK-15 and Vero cells. (A) Vero cell morphology in the presence of graphene oxide at different concentrations: (a) normal cells without GO, (b) 0.75, (c) 1.5, (d) 3, (e) 6, (f) 12.5, (g) 25, and (h) 50 μg/mL. Cell viability was measured by MTT. All the MTT values were normalized to the control (with no GO exposure), which represents 100% cell viability. (B) PK-15 cells; (C) Vero cells.

2.5. Western Blot. Cells in 6-well plates infected with PEDV in the presence or absence of GO were rinsed three times with PBS and then treated with lysis buffer (100 μL/well). Sodium dodecyl sulfate (SDS) loading buffer was added to the collected cell extracts and boiled for 10 min. Equivalent amounts of proteins were loaded and electrophoresed on 12% sodium dodecyl sulfate polyacrylamide gel electrophoresis (SDS-PAGE). Subsequently, the proteins were transferred to NC membranes followed by blocking with 5% skim milk for 2 h at 37 °C. The NC membranes were incubated with primary antibodies overnight at 4 °C and then exposed to HRP-conjugated secondary antibodies for 2 h at 37 °C.[14] The signals were collected using an enhanced chemiluminescence instrument. GAPDH was tested as a loading control.

2.6. Real-Time Quantitative PCR. After virus adsorption with an MOI of 0.01, cells were washed and incubated at 37 °C. The virus products were collected at 1, 5, 8, 12, 24, 36, and 48 h post infection. The viral DNA was extracted according to the manufacturer's instructions (OMEGA) and analyzed by quantitative real-time PCR on an ABI ViiA 7 real-time PCR system (Applied Biosystems, USA).[25]

2.7. Electron Microscopy. Supernatants of infected cells were collected and centrifuged at 4000 rpm for 30 min to remove cell debris. Then, the supernatants were ultracentrifuged at 26000 rpm for 2 h to obtain the virus resuspended in PBS. The purified virus was incubated with GO for 1 h at 37 °C followed by dropping on a copper grid for 10 min and then negatively staining with phosphotungstic acid (PTA, pH 7.0).[26] After drying, grids were examined using an electron microscope (Hitachi H7500).

3. RESULTS AND DISCUSSION

3.1. Characteristics of Graphene Oxide and Its Derivatives. Graphite (Gt), graphite oxide (GtO), graphene oxide (GO), reduced graphene oxide (rGO), graphene oxide/poly(diallyldimethylammonium chloride) composite (GO-PDDA), and graphene oxide/polyvinylpyrrolidone composite (GO-PVP) were prepared as described in the Supporting Information. Photographs and UV−vis absorbance spectra of the six dispersions listed above (at a concentration of 200 μg/mL) are shown in Figure 1A. As shown in the inset, the six materials presented different colors and dispersed states, which was attributed to their distinct structural and physicochemical properties. UV−vis absorbance spectra could further distinguish them. The changes of line Gt, GtO, and GO indicated that graphite was oxidized to GO with an absorption peak at ∼230 nm ($\pi \rightarrow \pi^*$) and a shoulder at ∼300 nm ($n \rightarrow \pi^*$) (Figure 1A).[27] After reduction by hydrazine hydrate, the previous two absorption peaks disappeared and a new absorption peak of rGO emerged at ∼260 nm, suggesting that GO was completely reduced and the electronic conjugation within the rGO sheets was restored upon N_2H_4 reduction.[28] If PVP or PDDA was decorated on GO, the absorption peak at ∼230 nm was not clear.

The Raman spectra (ELaser = 633 nm) of graphene-based nanomaterials are presented in Figure 1B. Raman spectroscopy is known as an efficient method to examine the ordered/disordered crystal structures of carbonaceous materials. The characteristic bands in the Raman spectra of carbons are located at around 1580 and 1350 cm^{-1}, corresponding to the graphite (G band, first-order scattering of E_{2g} phonons by sp^2 carbon atoms) and diamondoid bands (D band, breathing mode of κ-point photons of A_{1g} symmetry), respectively.[29] The different intensity ratios (I_D/I_G) of Gt, GtO, and GO demonstrated that graphene sheets changed to be more amorphous and defective upon exfoliation of Gt flakes. The D/G intensity ratio of rGO increased notably in comparison with that of GO, indicating an increase in the number of smaller graphitic domains upon reduction. Upon functionalization with PDDA or PVP, the G band of graphene up-shifted a little, further indicating the occurrence of electron transfer from graphene to the adsorbed PDDA or PVP.[30−33]

DOI: 10.1021/acsami.5b06876
ACS Appl. Mater. Interfaces 2015, 7, 21571−21579

Fourier transform infrared (FTIR) spectroscopy of GO showed a strong peak at around 1640 cm^{-1} attributable to aromatic C═C, along with peaks characteristic of O−H groups stretching vibration broad peak at ∼3450 cm^{-1}, C═O stretching vibration peak at around 1727 cm^{-1}, C−O stretching peak at ∼1052 cm^{-1}, carboxyl (∼1415 cm^{-1}), and epoxy (∼1226 cm^{-1}) (Figure S1).[34,35] GO-PDDA is reflected by the appearance of new peaks at around 850 and 1505 cm^{-1}, attributable to the N═C bond in the adsorbed PDDA. The spectrum of GO-PDDA also exhibits peaks at 2925, 1642, and 1467 cm^{-1}, belonging to the characteristic bands of PDDA.[36] Those characteristic peaks of PVP at ∼1646 cm^{-1} for C═O stretching at 1020, 1102, and 1291 cm^{-1} for the C−N vibration conformed the grafting of PVP from the GO surface.[37] Also, a broad peak comprising two peaks at 2875 and 2962 cm^{-1} with increased intensity is observed due to the presence of the CH_2 group in the PVP chain.[38]

The GO sheets had a ζ potential of −32.4 mV, indicating the presence of negatively charged groups in the GO structure (Figure S2). After reduction, the negative charge of rGO with a ζ potential of −26.4 mV was only a little less than that of GO. Besides, neutral polymer (PVP) and cationic polymer (PDDA) functionalized GO had a ζ potential of −31.1 mV and +34 mV, respectively.

The morphological differences between GO and rGO were further investigated by TEM presented in Figure 1. The exfoliated GO presented a flat ultrathin sheet structure due to the destruction of van der Waals interactions between GO layers upon sonication and the existence of a large amount of oxygen-containing functional groups on the surface of GO nanosheets. The rGO presented an analogous sheet structure with lots of wrinkles compared to GO. Atomic force microscopy (AFM) images of Gt, GtO, GO, and rGO deposited on a mica substrate were displayed to explore the thickness of each nanosheet (Figure 1E). GtO had a thickness of 7−9 nm attributable to multilayer structures of graphene oxide layers. The exfoliated GO sheets had a typical thickness of ∼1 nm, corresponding to the typical thickness of the single-layer graphene oxide sheets,[39] indicating that single-layer GO sheets were produced. Most of rGO sheets had the same thickness of ∼1 nm compared to that of GO sheets, indicating a reduction process could not lead to the stacking of graphene layers.

3.2. Toxicity of Graphene Oxide on Cells. Because the proliferation of viruses relies on host cells, it is important to ensure the antiviral activity of the nanomaterials did not result from a cytotoxic effect on the host cells. To determine the potential antiviral activity of GO and the proper concentration for the experiment, we first evaluated the viability of cells treated by GO in the concentration range from 1.5625 to 50 μg/mL for 72 h. As shown in Figure 2, GO showed similar toxicity on PK-15 and Vero cells. The cell viability was more than 90% when treated with GO at a concentration of 6 μg/mL. Meanwhile, the cell morphology was not affected at this concentration (Figure 2A). Thus, 6 μg/mL was chosen for the subsequent antiviral experiments.

3.3. Graphene Oxide Exhibits Antiviral Activity on PRV. To evaluate the antiviral potentials of graphene oxide against PRV, we infected PK-15 cells with PRV (2000 or 200 pfu/well) in the presence or absence of GO (6 μg/mL). As shown in Figure 3, the cells treated with 6 μg/mL of GO showed similar monolayer morphologies and viabilities to those of the mock-infected cells not treated with GO. The cell cultures had typical cytopathic effects in the absence of GO (Figure 3A). When treated with GO, the plaque formation unit was significantly

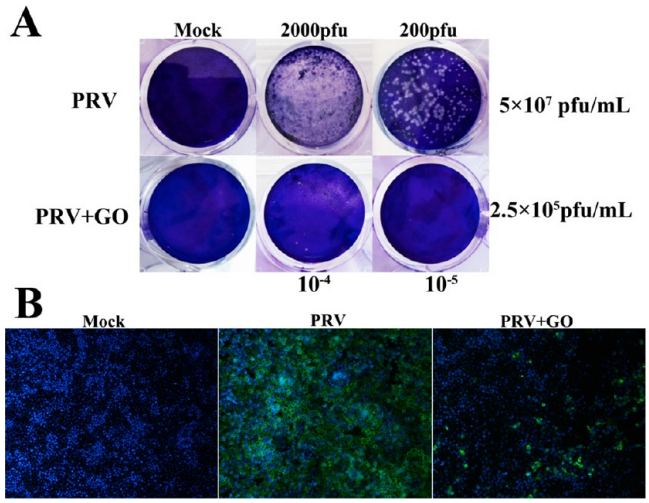

Figure 3. Anti-PRV activity of graphene oxide on PK-15 cells. (A) Plaque-reduction assay using PK-15 cells infected with PRV in the presence and absence of GO. The number of plaques (clear spots) observed represents the amount of virus in a given dilution. Mock-infected cells (top left); cells infected with PVR of 2000 pfu (top middle) and 200 pfu (top right); cells treated with 6 μg/mL GO (bottom left); PRV-infected cells in the presence of GO at 2000 pfu (bottom middle) and 200 pfu (bottom right). (B) Indirect immunofluorescence assay of PK-15 cells infected with PRV in the presence and absence of GO. Blue, DAPI; green, FITC-conjugated goat antimouse antibody.

decreased from 5×10^7 to 2.5×10^5 pfu/mL, indicating the inhibitory properties of GO.

To further confirm the result, we performed the inhibitory assay using an indirect immunofluorescence assay. PK-15 cells were infected with PRV at 0.01 MOI in the presence or absence of GO. After 24 h, the cells were fixed and immunostained with specific antibody against PRV gD protein. In accordance with the plaque-reduction assay, the number of PRV-infected cells (indicated by green fluorescence) in the absence of GO was significantly decreased compared that in the PRV-infected group (Figure 3B), indicating that GO blocked the viral infection. This result further demonstrated the efficient antiviral activity of GO against PRV.

3.4. Graphene Oxide Exhibits Antiviral Activity on PEDV. To explore the antiviral spectrum of graphene oxide, we applied another RNA virus, PEDV (a member of coronaviridae), to address the antiviral potential of GO. Similar to the results for PRV, GO (6 μg/mL) added before viral adsorption reduced the expression level of the PEDV viral protein and the plaque-forming ability as determined by Western blot analysis, plaque formation assays, and indirect immunofluorescence assays (Figure 4). Thus, graphene oxide possesses antiviral properties against both DNA and RNA viruses. Moreover, this broad spectrum antiviral activity was concentration- and time-dependent (Figure 5). The antiviral behavior was increased upon extending the incubation time and increasing the GO concentration. GO showed significant antiviral activity even at a low concentration of 1.5 μg/mL. Most of the virus inactivation occurred in the first hour of incubation. These results suggest that GO possesses time- and concentration-dependent antiviral properties against both DNA and RNA viruses.

3.5. Antivirial Activity of Graphene Oxide Is Associated with a Sharp-Edged Structure and Negative Charge. For better understanding of the antiviral mechanism of graphene

DOI: 10.1021/acsami.5b06876
ACS Appl. Mater. Interfaces 2015, 7, 21571−21579

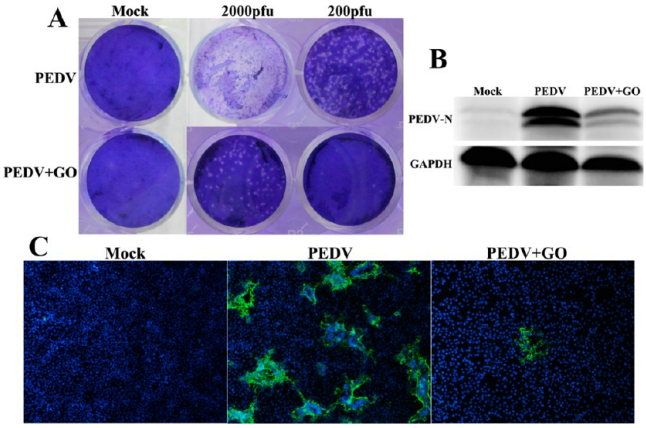

Figure 4. Anti-PEDV activity of graphene oxide on Vero cells. (A) Plaque-reduction assay using Vero cells infected with PEDV in the presence and absence of GO at 2000 and 200 pfu. (B) Western blot analysis of the expression level of PEDV-N protein when GO was added. GAPDH was used as a loading control. (C) Indirect immunofluorescence assay of PEDV-infected Vero cells. Blue, DAPI; green, FITC-conjugated goat antimouse antibody.

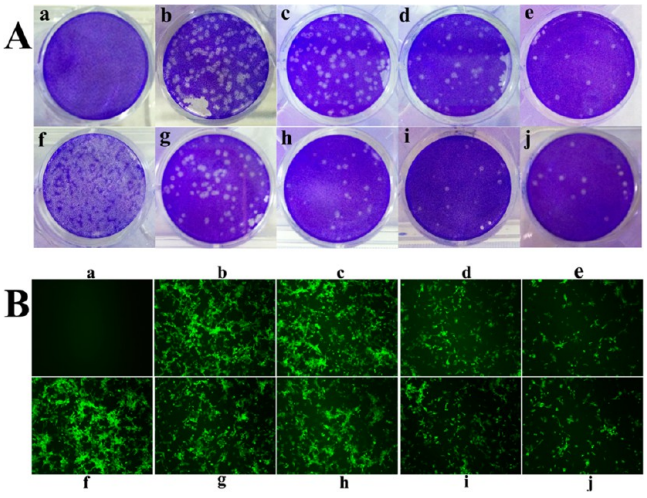

Figure 5. Antiviral behavior of GO at different time intervals and concentrations. (A) Time- and concentration-dependent anti-PRV activity of GO. (B) Fluorescence intensity of PEDV in the presence of GO at different times and concentrations: (a) mock-infected cells; (f) cells infected with viruses at 2000 pfu. The viruses were incubated with GO at 1.5 (b), 3 (c), 6 (d), and 12 μg/mL (e) for 1 h. The viruses were incubated with 6 μg/mL of GO for 10 (g), 30 (h), 60 (i), and 90 min (j).

oxide, six types of graphite-based materials (graphite (Gt), graphite oxide (GtO), graphene oxide (GO), reduced graphene oxide (rGO), GO-PDDA, and GO-PVP) were used to evaluate the antiviral activity. It is well-known that the surface chemistry of the nanoparticles plays an essential role in their interactions with external systems,[40] such as the various oxygen-containing groups on GO.[41] To test whether these functional groups play roles in antiviral properties, we reduced GO to explore whether there were any differences in the inhibition activity from GO. Beyond our expectations, rGO (Figure 6d) showed similar antiviral activity to that of GO (Figure 6c), indicating that the functional groups may not be essential for the antiviral activities. This finding is in agreement with a previous study.[21]

As indicated from zeta potential and AFM analysis, GO and rGO possess a similar negative charge (Figure S2) and single-layer structure (Figure 1E). Because GO and rGO both possess antiviral activity, we hypothesized that the sharp edge and negative charge are associated with the antiviral activity. Matias Sametband et al. demonstrated that GO and rGO−SO3 blocked HSV-1 infections, and they believe that the charge density is probably the dominant factor affecting the inhibition properties because the GO and rGO−SO3 have roughly the same ζ potential, but they did not demonstrate that through experiments.[21] We used PDDA, a cationic polymer, to test whether the negative charge of GO is responsible for its antiviral activity. The positively charged GO-PDDA exhibits no obvious antiviral activity (Figure 6e), indicating that the charge seems to be essential for its antiviral activity. On the other hand, the reason the GO-PDDA composite lost the antiviral activity may also be explained by the polymer wrap rather than the loss of negative charge. To test whether the negative charge or polymer wrap influences the antiviral activity of GO, we used another nonionic polymer, PVP, which has no influence on the charge. As shown in Figure 6f, GO-PVP also exhibited significant antiviral activity.

GO particles size was considered to be important for antibacterial activity.[42,43] Considering the changes in particle size upon polymer complexation, DLS was adopted to estimate the size distribution of GO-based materials. Particles size-distributed at 0.1−2 μm while the peak position was slightly different (Figure S4). GO-PDDA and GO-PVP had similar particle sizes, but GO-PVP rather than GO-PDDA exhibited antiviral activity, suggesting that particle size in our experimental condition did not influence antiviral activity. These results indicated that the negative charge has a greater influence on the antiviral activity of GO. It has been demonstrated that the surface coating of nanomaterials could improve the biocompatibility.[44,45] Zhi et al. demonstrated that PVP-coated GO possesses better immunological biocompatibility and immunoenhancement effects in vitro than GO.[46] Thus, polymer-coated (such as PVP), GO which has no influence on negative charge, may be a better candidate as an antimicrobial agent.

As precursors of GO, Gt and GtO were adopted to evaluate whether the single-layer structure has any effect on the antiviral activity. Viruses were incubated with the same concentration (6 μg/mL) of GO, rGO, Gt, and GtO for 1 h. Results showed that Gt exhibited no obvious antiviral properties (Figure 6g), whereas GtO (Figure 6f) showed a much weaker antiviral activity than GO or rGO. Significant differences were found in the antiviral activities among these materials (Figure 6B), which may be attributed to their different nanosheet structures. The AFM results indicated that the GtO has a much larger height than GO or rGO (Figure 1), which may contribute to the much weaker antiviral activity of GtO, whereas Gt showed no nanosheet structure or antiviral properties. This structure-dependent toxicity in graphite derivatives is in accordance with a previous study.[47] Liu et al. have previously demonstrated that GO has higher cytotoxicity toward *E. coli* than Gt or GtO.[47] It can be inferred from these GO-based materials that the antiviral properties are closely related to the nanosheet structure.

These results are consistent with each other on both PRV (Figure 6A) and PEDV (Figure 6C) evaluated by different experimental methods (plaque reduction assay and fluorescence). Taken together, the unique nanosheet structure and the negative charge could account for the antiviral activity of GO and rGO.

3.6. Graphene Oxide Inactivates Virus Particles Prior to Cell Entry. Each stage of virus infection represents a possible target for inhibition.[48] To determine the stage at which the virus

DOI: 10.1021/acsami.5b06876
ACS Appl. Mater. Interfaces 2015, 7, 21571−21579

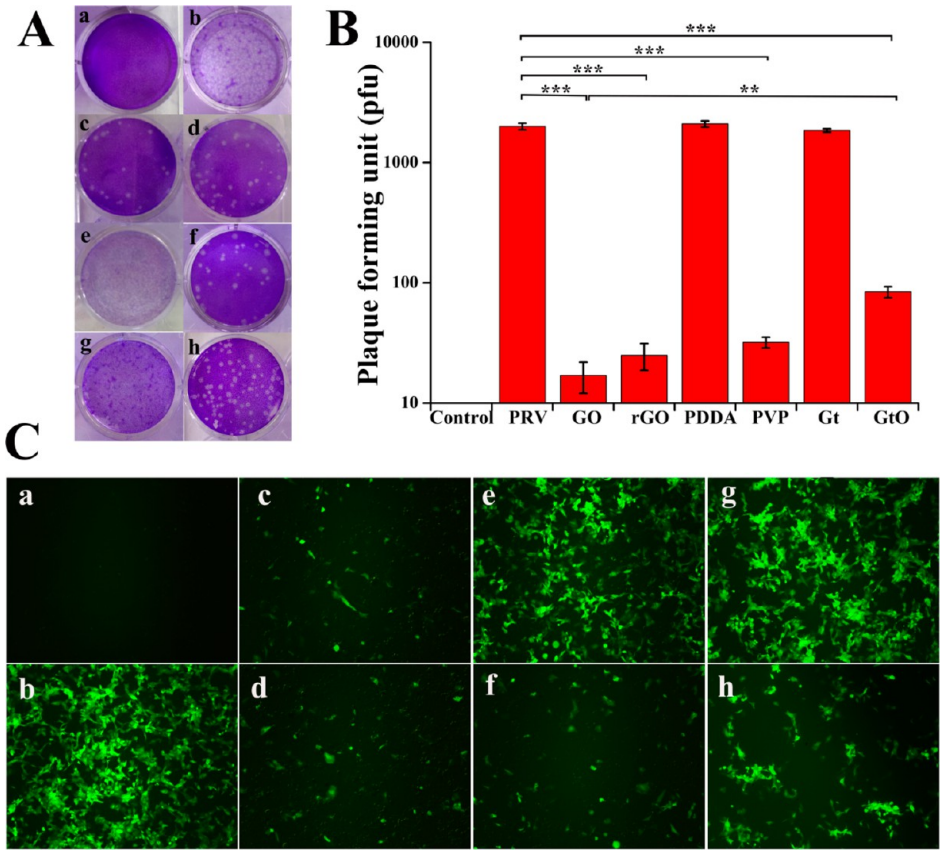

Figure 6. Antiviral activity of graphene oxide-based materials. (A) Plaque-reduction assay of PRV in the absence (b) or presence of GO (c), rGO (d), GO-PDDA (e), GO-PVP (f), Gt (g), and GtO (h). (B) Plaque-formation analysis of (A). The results are presented as the mean ± SD of three independent experiments. The statistical analysis was performed using SPSS statistics 17.0:; significance was defined as $P < 0.05$ (*), and high significance was defined as $P < 0.01$ (**) and $P < 0.001$ (***). (C) Fluorescence of PEDV treated with the same GO-based materials as those for PRV. (a) Mock-infected cells.

infection was blocked by GO, different treatments were used for the addition of GO to cells: (i) incubation with cells for 1 h before virus adsorption, (ii) preincubation with the virus for 1 h, (iii) simultaneous incubation with the virus adsorption, and (iv) after virus adsorption for 1 h. A recombinant PEDV strain containing a green fluorescent protein (GFP) cassette, DR13-GFP, was used for real-time monitoring of the infected cells. The fluorescence of infected cells treated with GO before (Figure 7Ad), after (Figure 7Ae), and simultaneously with (Figure 7Af) the virus adsorption showed no significant difference from that of the infected cells without GO (Figure 7Ab). The results showed that only preincubation of virus with GO exhibited significant inhibition of infection (Figure 7Ac). The presence of GO in cell culture did not block the viral replication and spread to neighboring cells. We suggest that GO inhibits virus infection by inactivating the virus particles prior to entry into the cell.

To further confirm this proposition, we conducted the same treatment assay on PK-15 cells infected with PRV. The virus products were collected separately at 1, 4, 8, 12, 24, 36, and 48 h to determine the viral growth curve under different protocols by quantitative real-time PCR. As shown in Figure 7B, PRV infections on PK-15 cells were also blocked only by preincubation with GO for 1 h. This finding is in agreement with the observation on Vero cells. Moreover, after 1 h virus adsorption at each group, cells were washed 3 times with PBS, and the viral products were collected for quantitative real-time PCR to examine the virus adsorption under different treatments. As shown in Figure 7B, the virus titer of each protocol showed no difference at the first time point (1 h), implying that GO did not affect virus adsorption. The observation of an antiviral effect only from the preincubation before viral adsorption suggests that GO blocks virus infection mainly at the stage before viral entry rather than post virus entry.

3.7. Viral Morphology Is Destroyed by the Sharp Edge of GO. As implied by the aforementioned results, GO may inhibit virus infection by direct interaction with the virus, resulting in virus inactivation by the sharp-edged structure. To further confirm this assumption, we incubated the extracted viral particles in the supernatant of infected cells with GO and negatively stained them to reveal the interaction between GO and the virus. Mature PRV virions consist of a nucleocapsid surrounded by the tegument and the envelope. The envelope contains numerous glycoprotein spikes.[49−52] Typically, spherical virial particles with integrated envelopes and spikes have been observed by electron microscopy (Figure 8A). After incubation with GO for 1 h, part of the envelope and spikes were destroyed (Figure 8B). The same viral morphology damage was observed in PEDV. As shown in Figure 8C, PEDV particles are round to pleomorphic particles surrounded by a crownlike corona.[53−55] However, after incubation with GO, the crown and the envelope were destroyed (Figure 8D). These results show that GO could directly interact with viral particles and destroy their structures, leading to the disruption of viral function. In a previous study, GO nanowalls were found to inactivate bacteria by direct contact of the bacteria with the sharp edges of the nanowalls.[56] GO nanosheets can also penetrate into cell membranes of bacteria

DOI: 10.1021/acsami.5b06876
ACS Appl. Mater. Interfaces 2015, 7, 21571−21579

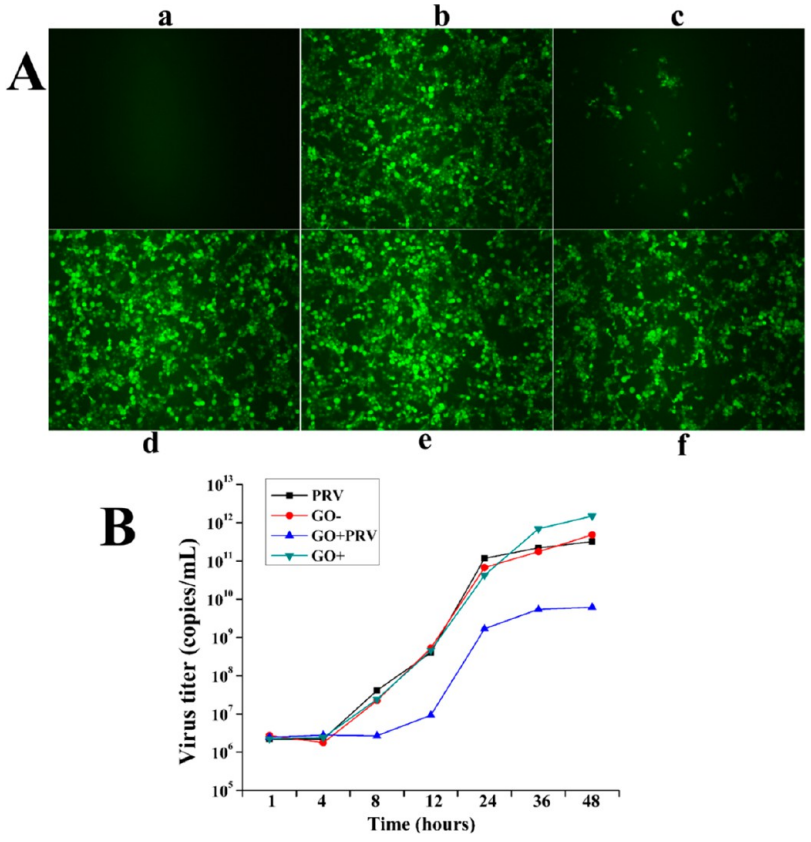

Figure 7. GO treatments at different stages of viral infection. (A) Live image of Vero cells infected with GFP-expressing PEDV strain. (a) Mock-infected cells; (b) GFP-expressing PEDV-infected cells; (c) virus preincubated with GO for 1 h before virus attachment; (d) GO added 1 h before virus attachment; (e) GO added after 1 h adsorption; and (f) GO added simultaneously with virus. (B) Quantitative real-time PCR of PK-15 cells infected with PRV at different treatments of GO. The red line (GO−) means GO was added 1 h before virus attachment. The blue line (GO+PRV) shows the result of preincubation of GO and PRV. The green line (GO+) means GO was added 1 h after virus adsorption.

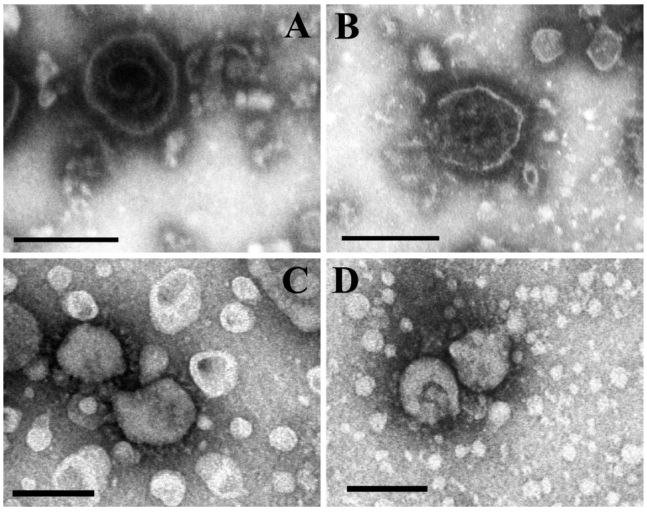

Figure 8. Transmission electron microscopic images of GO-treated viruses. (A) PRV control; (B) PRV treated with GO for 1 h; (C) PEDV control; and (D) PEDV incubated with GO for 1 h. Scale bars: 200 nm (A, B) and 100 nm (C, D).

and extract phospholipids.[57] Destruction of viral morphology suggested that GO may inactivate the virus by using its sharp edge as well.

In addition to causing damage through their sharp edges, GO (and rGO) particles are widely considered to inhibit bacterial cells through wrapping.[42] PRV and PEDV are spherical viruses approximately 200 and 100 nm in diameter. The GO used in this study are ~500 nm in size (Figure S4). Thus, the wrapping effect might be relevant for GO.

Additionally, viral electrostatic charge played major roles in the virus infection process.[58] Liang et al. found that the electrostatic interaction between the negatively charged nanoscale silicate platelet and the positively charged virus particles blocks viral binding.[59] The positively charged virus particles may adsorb to negatively charged GO, which perhaps is the reason why positively charged GO-PDDA loses antiviral activity.

4. CONCLUSIONS

In the present study, we demonstrated that GO and rGO exhibit broad-spectrum antiviral activity toward both DNA virus (PRV) and RNA virus (PEDV) at a noncytotoxic concentration (6 μg/mL). This antiviral activity is time- and concentration-dependent. GO exhibits significant antiviral properties even at a low concentration (1.5 μg/mL). The antiviral mechanism of GO may be attributed to the negative charge and nanosheet structure. Both GO and rGO show similar antiviral activity, indicating that the oxygen-containing group is not essential for the antiviral activity. The cationic GO-PDDA has no antiviral activity, but the nonionic GO-PVP shows similar antiviral activity as GO, which is consistent with our hypothesis that the negative charge is required for the antiviral mechanism of GO and rGO. The polylaminate GtO shows much weaker antiviral activity than single-layered GO and rGO, whereas the non-nanosheet Gt

DOI: 10.1021/acsami.5b06876
ACS Appl. Mater. Interfaces 2015, 7, 21571−21579

shows no antiviral activity, suggesting that the nanosheet structure is important for the antiviral activity. Moreover, the GO was added to the cell culture at different stages of viral infection to determine at which stage GO works. GO exhibits antiviral activity only when incubated with virus prior to viral adsorption but does not work after or even simultaneously with the onset of viral infection. GO inactivates the viral particles prior to their entry into cells. The electrostatic interaction offers the negatively charged sharp-edged GO more chances to interact with the positively charged virus particles, resulting in virus destruction and inactivation.

This is most likely the first report on the antiviral spectrum with a proposal for a potential antiviral mechanism of GO. The broad-spectrum antiviral activity of GO and rGO may shed some light on novel virucide development.

■ ASSOCIATED CONTENT

Supporting Information

The Supporting Information is available free of charge on the ACS Publications website at DOI: 10.1021/acsami.5b06876.

Reagents, apparatuses, fabrication of GO-based materials, FTIR spectra, Zeta potentials, size distributions, and AFM characterizations (PDF)

■ AUTHOR INFORMATION

Corresponding Authors

*Tel: +86 027-87286974; Fax: +86 027-87282608; E-mail: he628@mail.hzau.edu.cn.

*Tel: +86 027-87288505; Fax: +86 027-87288505; E-mail: hyhan@mail.hzau.edu.cn.

Notes

The authors declare no competing financial interest.

■ ACKNOWLEDGMENTS

This work was financially supported by grants from the National Natural Sciences Foundation of China (21375043, 21175051) and the China Agricultural Research System (No. CARS-36).

■ REFERENCES

(1) Tomori, O. From Smallpox Eradication to the Future of Global Health: Innovations, Application and Lessons for Future Eradication and Control Initiatives. *Vaccine* **2011**, *29*, D145−D148.

(2) Gentsch, J. R.; Laird, A. R.; Bielfelt, B.; Griffin, D. D.; Bányai, K.; Ramachandran, M.; Jain, V.; Cunliffe, N. A.; Nakagomi, O.; Kirkwood, C. D. Serotype Diversity and Reassortment between Human and Animal Rotavirus Strains: Implications for Rotavirus Vaccine Programs. *J. Infect. Dis.* **2005**, *192*, S146−S159.

(3) Upadhyaya, S.; Ayelet, G.; Paul, G.; King, D. P.; Paton, D. J.; Mahapatra, M. Genetic Basis of Antigenic Variation in Foot-and-Mouth Disease Serotype A Viruses from the Middle East. *Vaccine* **2014**, *32* (5), 631−638.

(4) Li, W.; Li, H.; Liu, Y.; Pan, Y.; Deng, F.; Song, Y.; Tang, X.; He, Q. New Variants of Porcine Epidemic Diarrhea Virus, China, 2011. *Emerging Infect. Dis.* **2012**, *18* (8), 1350−1353.

(5) An, T.-Q.; Peng, J.-M.; Tian, Z.-J.; Zhao, H.-Y.; Li, N.; Liu, Y.-M.; Chen, J.-Z.; Leng, C.-L.; Sun, Y.; Chang, D. Pseudorabies Virus Variant in Bartha-K61−Vaccinated Pigs, China, 2012. *Emerging Infect. Dis.* **2013**, *19* (11), 1749−1755.

(6) Zhang, C.; Guo, L.; Jia, X.; Wang, T.; Wang, J.; Sun, Z.; Wang, L.; Li, X.; Tan, F.; Tian, K. Construction of a Triple Gene-Deleted Chinese Pseudorabies Virus Variant and Its Efficacy Study as a Vaccine Candidate on Suckling Piglets. *Vaccine* **2015**, *33* (21), 2432−2437.

(7) Wang, C.-H.; Yuan, J.; Qin, H.-Y.; Luo, Y.; Cong, X.; Li, Y.; Chen, J.; Li, S.; Sun, Y.; Qiu, H.-J. A Novel gE-deleted Pseudorabies Virus (PRV) Provides Rapid and Complete Protection from Lethal Challenge with the PRV Variant Emerging in Bartha-K61-Vaccinated Swine Population in China. *Vaccine* **2014**, *32* (27), 3379−3385.

(8) Luo, Y.; Li, N.; Cong, X.; Wang, C.-H.; Du, M.; Li, L.; Zhao, B.; Yuan, J.; Liu, D.-D.; Li, S.; Li, Y.; Sun, Y.; Qiu, H.-J. Pathogenicity and Genomic Characterization of a Pseudorabies Virus Variant Isolated from Bartha-K61-Vaccinated Swine Population in China. *Vet. Microbiol.* **2014**, *174* (1−2), 107−115.

(9) Wang, L.; Byrum, B.; Zhang, Y. New Variant of Porcine Epidemic Diarrhea Virus, United States, 2014. *Emerging Infect. Dis.* **2014**, *20* (5), 917−919.

(10) Chen, Q.; Li, G.; Stasko, J.; Thomas, J. T.; Stensland, W. R.; Pillatzki, A. E.; Gauger, P. C.; Schwartz, K. J.; Madson, D.; Yoon, K.-J. Isolation and Characterization of Porcine Epidemic Diarrhea Viruses Associated with the 2013 Disease Outbreak among Swine in the United States. *J. Clin. Microbiol.* **2014**, *52* (1), 234−243.

(11) Mao, H. Y.; Laurent, S.; Chen, W.; Akhavan, O.; Imani, M.; Ashkarran, A. A.; Mahmoudi, M. Graphene: Promises, Facts, Opportunities, and Challenges in Nanomedicine. *Chem. Rev.* **2013**, *113* (5), 3407−3424.

(12) Xiu, Z.-m.; Zhang, Q.-b.; Puppala, H. L.; Colvin, V. L.; Alvarez, P. J. Negligible Particle-Specific Antibacterial Activity of Silver Nanoparticles. *Nano Lett.* **2012**, *12* (8), 4271−4275.

(13) Li, Y.; Zhang, W.; Niu, J.; Chen, Y. Mechanism of Photogenerated Reactive Oxygen Species and Correlation with the Antibacterial Properties of Engineered Metal-Oxide Nanoparticles. *ACS Nano* **2012**, *6* (6), 5164−5173.

(14) Lv, X. N.; Wang, P.; Bai, R.; Cong, Y. Y.; Suo, S.; Ren, X. F.; Chen, C. Y. Inhibitory Effect of Silver Nanomaterials on Transmissible Virus-Induced Host Cell Infections. *Biomaterials* **2014**, *35* (13), 4195−4203.

(15) Prucek, R.; Tuček, J.; Kilianová, M.; Panáček, A.; Kvítek, L.; Filip, J.; Kolář, M.; Tománková, K.; Zbořil, R. The Targeted Antibacterial and Antifungal Properties of Magnetic Nanocomposite of Iron Oxide and Silver Nanoparticles. *Biomaterials* **2011**, *32* (21), 4704−4713.

(16) Geim, A. K.; Novoselov, K. S. The Rise of Graphene. *Nat. Mater.* **2007**, *6* (3), 183−191.

(17) He, J.; Zhu, X.; Qi, Z.; Wang, C.; Mao, X.; Zhu, C.; He, Z.; Li, M.; Tang, Z. Killing Dental Pathogens Using Antibacterial Graphene Oxide. *ACS Appl. Mater. Interfaces* **2015**, *7* (9), 5605−5611.

(18) Hu, W.; Peng, C.; Luo, W.; Lv, M.; Li, X.; Li, D.; Huang, Q.; Fan, C. Graphene-Based Antibacterial Paper. *ACS Nano* **2010**, *4* (7), 4317−4323.

(19) Chen, J.; Peng, H.; Wang, X.; Shao, F.; Yuan, Z.; Han, H. Graphene Oxide Exhibits Broad-Spectrum Antimicrobial Activity Against Bacterial Phytopathogens and Fungal Conidia by Intertwining and Membrane Perturbation. *Nanoscale* **2014**, *6* (3), 1879−1889.

(20) Li, C.; Wang, X.; Chen, F.; Zhang, C.; Zhi, X.; Wang, K.; Cui, D. The Antifungal Activity of Graphene Oxide−Silver Nanocomposites. *Biomaterials* **2013**, *34* (15), 3882−3890.

(21) Sametband, M.; Kalt, I.; Gedanken, A.; Sarid, R. Herpes Simplex Virus Type-1 Attachment Inhibition by Functionalized Graphene Oxide. *ACS Appl. Mater. Interfaces* **2014**, *6* (2), 1228−1235.

(22) Cheng, S.; Yan, W.; Gu, W.; He, Q. The Ubiquitin-Proteasome System is Required for the Early Stages of Porcine Circovirus Type 2 Replication. *Virology* **2014**, *456*, 198−204.

(23) Hsuan, S.-L.; Chang, S.-C.; Wang, S.-Y.; Liao, T.-L.; Jong, T.-T.; Chien, M.-S.; Lee, W.-C.; Chen, S.-S.; Liao, J.-W. The Cytotoxicity to Leukemia Cells and Antiviral Effects of Isatis Indigotica Extracts on Pseudorabies Virus. *J. Ethnopharmacol.* **2009**, *123* (1), 61−67.

(24) Zeng, S.; Zhang, H.; Ding, Z.; Luo, R.; An, K.; Liu, L.; Bi, J.; Chen, H.; Xiao, S.; Fang, L. Proteome Analysis of Porcine Epidemic Diarrhea Virus (PEDV)-Infected Vero Cells. *Proteomics* **2015**, *15* (11), 1819−1828.

(25) Matundan, H.; Mott, K. R.; Ghiasi, H. Role of CD8(+) T Cells and Lymphoid Dendritic Cells in Protection from Ocular Herpes Simplex Virus 1 Challenge in Immunized Mice. *J. Virol.* **2014**, *88* (14), 8016−8027.

(26) Chen, N.; Zheng, Y.; Yin, J.; Li, X.; Zheng, C. Inhibitory Effects of Silver Nanoparticles Against Adenovirus Type 3 in Vitro. *J. Virol. Methods* **2013**, *193* (2), 470−477.
(27) Paredes, J. I.; Villar-Rodil, S.; Martinez-Alonso, A.; Tascon, J. M. D. Graphene Oxide Dispersions in Organic Solvents. *Langmuir* **2008**, *24* (19), 10560−10564.
(28) Li, D.; Mueller, M. B.; Gilje, S.; Kaner, R. B.; Wallace, G. G. Processable Aqueous Dispersions of Graphene Nanosheets. *Nat. Nanotechnol.* **2008**, *3* (2), 101−105.
(29) Fan, Z.-J.; Kai, W.; Yan, J.; Wei, T.; Zhi, L.-J.; Feng, J.; Ren, Y.-m.; Song, L.-P.; Wei, F. Facile Synthesis of Graphene Nanosheets via Fe Reduction of Exfoliated Graphite Oxide. *ACS Nano* **2011**, *5* (1), 191−198.
(30) Wang, S.; Yu, D.; Dai, L.; Chang, D. W.; Baek, J.-B. Polyelectrolyte-Functionalized Graphene as Metal-Free Electrocatalysts for Oxygen Reduction. *ACS Nano* **2011**, *5* (8), 6202−6209.
(31) Eklund, P. C.; Rao, A. M.; Bandow, S.; Thess, A.; Smalley, R. E. Evidence for Charge Transfer in Doped Carbon Nanotube Bundles from Raman Scattering. *Nature* **1997**, *388*, 257−259.
(32) Qi, X.; Pu, K.-Y.; Zhou, X.; Li, H.; Liu, B.; Boey, F.; Huang, W.; Zhang, H. Conjugated-Polyelectrolyte-Functionalized Reduced Graphene Oxide with Excellent Solubility and Stability in Polar Solvents. *Small* **2010**, *6* (5), 663−669.
(33) Hsiao, M.-C.; Liao, S.-H.; Yen, M.-Y.; Liu, P.-I.; Pu, N.-W.; Wang, C.-A.; Ma, C.-C. M. Preparation of Covalently Functionalized Graphene Using Residual Oxygen-Containing Functional Groups. *ACS Appl. Mater. Interfaces* **2010**, *2* (11), 3092−3099.
(34) Zhang, J.; Yang, H.; Shen, G.; Cheng, P.; Zhang, J.; Guo, S. Reduction of Graphene Oxide via L-Ascorbic Acid. *Chem. Commun.* **2010**, *46* (7), 1112−1114.
(35) Ahmad, M.; Ahmed, E.; Hong, Z. L.; Xu, J. F.; Khalid, N. R.; Elhissi, A.; Ahmed, W. A Facile One-Step Approach to Synthesizing ZnO/Graphene Composites for Enhanced Degradation of Methylene Blue under Visible Light. *Appl. Surf. Sci.* **2013**, *274*, 273−281.
(36) Liu, L.; Gao, X.; Zhang, P.; Feng, S.-l.; Hu, F.-d.; Li, Y.-d.; Wang, C.-m. Ultrasensitive Detection of Ferulic Acid Using Poly-(diallyldimethylammonium chloride) Functionalized Graphene-Based Electrochemical Sensor. *J. Anal. Methods Chem.* **2014**, *2014*, 1−9.
(37) Wang, H. S.; Qiao, X. L.; Chen, J. G.; Wang, X. J.; Ding, S. Y. Mechanisms of PVP in the Preparation of Silver Nanoparticles. *Mater. Chem. Phys.* **2005**, *94* (2−3), 449−453.
(38) Layek, R. K.; Kuila, A.; Chatterjee, D. P.; Nandi, A. K. Amphiphilic poly(N-vinyl pyrrolidone) Grafted Graphene by Reversible Addition and Fragmentation Polymerization and the Reinforcement of Poly(vinyl acetate) Films. *J. Mater. Chem. A* **2013**, *1* (36), 10863−10874.
(39) Schniepp, H. C.; Li, J. L.; McAllister, M. J.; Sai, H.; Herrera-Alonso, M.; Adamson, D. H.; Prud'homme, R. K.; Car, R.; Saville, D. A.; Aksay, I. A. Functionalized Single Graphene Sheets Derived from Splitting Graphite Oxide. *J. Phys. Chem. B* **2006**, *110* (17), 8535−8539.
(40) Das, S.; Singh, S.; Singh, V.; Joung, D.; Dowding, J. M.; Reid, D.; Anderson, J.; Zhai, L.; Khondaker, S. I.; Self, W. T.; Seal, S. Oxygenated Functional Group Density on Graphene Oxide: Its Effect on Cell Toxicity. *Part. Part. Syst. Charact.* **2013**, *30* (2), 148−157.
(41) Yang, K.; Wan, J.; Zhang, S.; Tian, B.; Zhang, Y.; Liu, Z. The Influence of Surface Chemistry and Size of Nanoscale Graphene Oxide on Photothermal Therapy of Cancer Using Ultra-Low Laser Power. *Biomaterials* **2012**, *33* (7), 2206−2214.
(42) Liu, S.; Hu, M.; Zeng, T. H.; Wu, R.; Jiang, R.; Wei, J.; Wang, L.; Kong, J.; Chen, Y. Lateral Dimension-Dependent Antibacterial Activity of Graphene Oxide Sheets. *Langmuir* **2012**, *28* (33), 12364−12372.
(43) Perreault, F.; de Faria, A. F.; Nejati, S.; Elimelech, M. Antimicrobial Properties of Graphene Oxide Nanosheets: Why Size Matters. *ACS Nano* **2015**, *9* (7), 7226−7236.
(44) Yang, K.; Feng, L.; Shi, X.; Liu, Z. Nano-Graphene in Biomedicine: Theranostic Applications. *Chem. Soc. Rev.* **2013**, *42* (2), 530−547.
(45) Li, B.; Zhang, X.-Y.; Yang, J.-Z.; Zhang, Y.-J.; Li, W.-X.; Fan, C.-H.; Huang, Q. Influence of Polyethylene Glycol Coating on Biodistribution and Toxicity of Nanoscale Graphene Oxide in Mice after Intravenous Injection. *Int. J. Nanomed.* **2014**, *9*, 4697−4707.
(46) Zhi, X.; Fang, H.; Bao, C.; Shen, G.; Zhang, J.; Wang, K.; Guo, S.; Wan, T.; Cui, D. The Immunotoxicity of Graphene Oxides and the Effect of PVP-Coating. *Biomaterials* **2013**, *34* (21), 5254−5261.
(47) Liu, S.; Zeng, T. H.; Hofmann, M.; Burcombe, E.; Wei, J.; Jiang, R.; Kong, J.; Chen, Y. Antibacterial Activity of Graphite, Graphite Oxide, Graphene Oxide, and Reduced Graphene Oxide: Membrane and Oxidative Stress. *ACS Nano* **2011**, *5* (9), 6971−6980.
(48) Baram-Pinto, D.; Shukla, S.; Gedanken, A.; Sarid, R. Inhibition of HSV-1 Attachment, Entry, and Cell-to-Cell Spread by Functionalized Multivalent Gold Nanoparticles. *Small* **2010**, *6* (9), 1044−1050.
(49) Grunewald, K.; Desai, P.; Winkler, D. C.; Heymann, J. B.; Belnap, D. M.; Baumeister, W.; Steven, A. C. Three-Dimensional Structure of Herpes Simplex Virus from Cryo-Electron Tomography. *Science* **2003**, *302* (5649), 1396−1398.
(50) Granzow, H.; Klupp, B. G.; Fuchs, W.; Veits, J.; Osterrieder, N.; Mettenleiter, T. C. Egress of Alphaherpesviruses: Comparative Ultrastructural Study. *J. Virol.* **2001**, *75* (8), 3675−3684.
(51) Pomeranz, L. E.; Reynolds, A. E.; Hengartner, C. J. Molecular Biololgy of Pseudorabies Virus: Impact on Neurovirology and Veterinary Medicine. *Microbiol. Mol. Biol. Rev.* **2005**, *69* (3), 462−500.
(52) Klupp, B.; Altenschmidt, J.; Granzow, H.; Fuchs, W.; Mettenleiter, T. C. Glycoproteins Required for Entry are not Necessary for Egress of Pseudorabies Virus. *J. Virol.* **2008**, *82* (13), 6299−6309.
(53) Hofmann, M.; Wyler, R. Propagation of the Virus of Porcine Epidemic Diarrhea in Cell Culture. *J. Clin. Microbiol.* **1988**, *26* (11), 2235−2239.
(54) Oka, T.; Saif, L. J.; Marthaler, D.; Esseili, M. A.; Meulia, T.; Lin, C.-M.; Vlasova, A. N.; Jung, K.; Zhang, Y.; Wang, Q. Cell Culture Isolation and Sequence Analysis of Genetically Diverse US Porcine Epidemic Diarrhea Virus Strains Including a Novel Strain with a Large Deletion in the Spike Gene. *Vet. Microbiol.* **2014**, *17*, 258−269.
(55) Song, D.; Park, B. Porcine Epidemic Diarrhoea Virus: a Comprehensive Review of Molecular Epidemiology, Diagnosis, and Vaccines. *Virus Genes* **2012**, *44* (2), 167−175.
(56) Akhavan, O.; Ghaderi, E. Toxicity of Graphene and Graphene Oxide Nanowalls Against Bacteria. *ACS Nano* **2010**, *4* (10), 5731−5736.
(57) Tu, Y.; Lv, M.; Xiu, P.; Huynh, T.; Zhang, M.; Castelli, M.; Liu, Z.; Huang, Q.; Fan, C.; Fang, H.; Zhou, R. Destructive Extraction of Phospholipids from Escherichia Coli Membranes by Graphene Nanosheets. *Nat. Nanotechnol.* **2013**, *8* (8), 594−601.
(58) Michen, B.; Graule, T. Isoelectric Points of Viruses. *J. Appl. Microbiol.* **2010**, *109* (2), 388−397.
(59) Liang, J.-J.; Wei, J.-C.; Lee, Y.-L.; Hsu, S.-h.; Lin, J.-J.; Lin, Y.-L. Surfactant-Modified Nanoclay Exhibits an Antiviral Activity with High Potency and Broad Spectrum. *J. Virol.* **2014**, *88* (8), 4218−4228.

DOI: 10.1021/acsami.5b06876
ACS Appl. Mater. Interfaces 2015, 7, 21571−21579